

## Article

# Mineralogy of the Steel Mountain Anorthosite Complex, Western Newfoundland Appalachians, Canada: Petrogenesis and Tectonic Affinity

Georgia Pe-Piper <sup>1,\*</sup>, David J. W. Piper <sup>2</sup> and Gilles Dessureau <sup>1,3</sup><sup>1</sup> Department of Geology, Saint Mary's University, Halifax, NS B3H 3C3, Canada; gillesd@solidusgeo.com<sup>2</sup> Natural Resources Canada, Geological Survey of Canada Atlantic, Bedford Institute of Oceanography, Dartmouth, NS B2Y 4A2, Canada; david.piper@canada.ca<sup>3</sup> Solidus Geological Services, 308-3131 Main St., Vancouver, BC V5T 3G8, Canada

\* Correspondence: gpiper@smu.ca

**Abstract:** The Steel Mountain complex in western Newfoundland is one of several possible peri-Gondwanan basement slivers that have been emplaced along the northwestern margin of the Appalachian Orogen. The complex includes feldspathic anorthosite, gabbro-norite, and magnetite-ilmenite ore. Megacrysts of plagioclase (andesine), orthopyroxene (hypersthene) and amphibole (hornblende) were analyzed by electron microprobe and they are of similar composition to the groundmass minerals. The ferromagnesian megacrysts have exsolution lamellae of Fe-Ti oxides, magnesio-hornblende, and clinopyroxene. The hornblende megacrysts and the lack of plagioclase in the exsolution lamellae are unusual for Proterozoic anorthosites and result from unusual abundance of water in the parental magma. Whole-rock Nd-Sm isotope determinations give an isochron age of ~1.2 Ga. Ar-Ar dating of biotite rims on hornblende shows an early Ordovician plateau age and the final heating step suggests a ~0.8 Ga age for the amphibole itself. Taken together with published zircon geochronology, these data suggest a provenance in the southern peri-Gondwanan Appalachians.

**Keywords:** anorthosite; Proterozoic; Newfoundland; mineral chemistry; geochronology; petrogenesis



**Citation:** Pe-Piper, G.; Piper, D.J.W.; Dessureau, G. Mineralogy of the Steel Mountain Anorthosite Complex, Western Newfoundland Appalachians, Canada: Petrogenesis and Tectonic Affinity. *Minerals* **2024**, *14*, 81. <https://doi.org/10.3390/min14010081>

Academic Editor: Jean-Michel Lafon

Received: 29 November 2023

Revised: 22 December 2023

Accepted: 28 December 2023

Published: 11 January 2024



**Copyright:** © 2024 by the authors and by His Majesty the King in Right of Canada, as represented by the Minister of Natural Resources. Submitted for possible open access publication under the terms and conditions of the Creative Commons Attribution (CC BY) license (<https://creativecommons.org/licenses/by/4.0/>).

## 1. Introduction

Several Proterozoic inliers crop out along the northwestern margin of the Appalachian Orogen in western Newfoundland, Canada (Figure 1). The original palinspastic position of these inliers is controversial and they may have moved great distances along strike slip faults [1]. The Steel Mountain complex, near the town of Corner Brook, is exceptional in being an anorthosite massif, some 50 km long. The age of the Steel Mountain complex is unresolved. U-Pb analysis of zircons has yielded ages of ~1.14 and ~0.6 Ga ages [2], as well as one poor quality 1.27 Ga age [3].

Proterozoic anorthosites have been recently reviewed by [4]. They comprise principally plagioclase feldspar, commonly megacrystic, with lesser amounts of orthopyroxene [5]. Associated rocks with greater amounts of ferromagnesian minerals are gabbro-norites. Geobarometric estimates based on orthopyroxene suggest polybaric crystallization over a range of lower- and middle-crustal depths [6]. Proterozoic anorthosite massifs were built by multiple intrusions of andesine-labradorite-rich crystal mushes, derived from a deeper parental basaltic magma, perhaps in an Andean-type margin, and the plate dynamics at such margins are postulated to have been different in the Proterozoic Eon compared to the Phanerozoic Eon [4]. In general, indications of hydrous magma are rare in Proterozoic anorthosites, although rare amphibole has been reported, mostly as inclusions in orthopyroxene [7–10].

The Steel Mountain complex includes anorthosite *sensu stricto*, gabbro-norite, and ilmenite-magnetite ore. Unlike most Proterozoic anorthosites, amphibole is common with

some as megacrysts. The purpose of this paper is two-fold. (1) To describe and interpret the unusual evidence for hydrous conditions in the evolution of the Steel Mountain anorthosite. (2) To use Nd-Sm isotopes,  $^{40}\text{Ar}$ - $^{39}\text{Ar}$  geochronology, and the mode of occurrence of zircon to further constrain the age and tectonic history of the anorthosite massif.

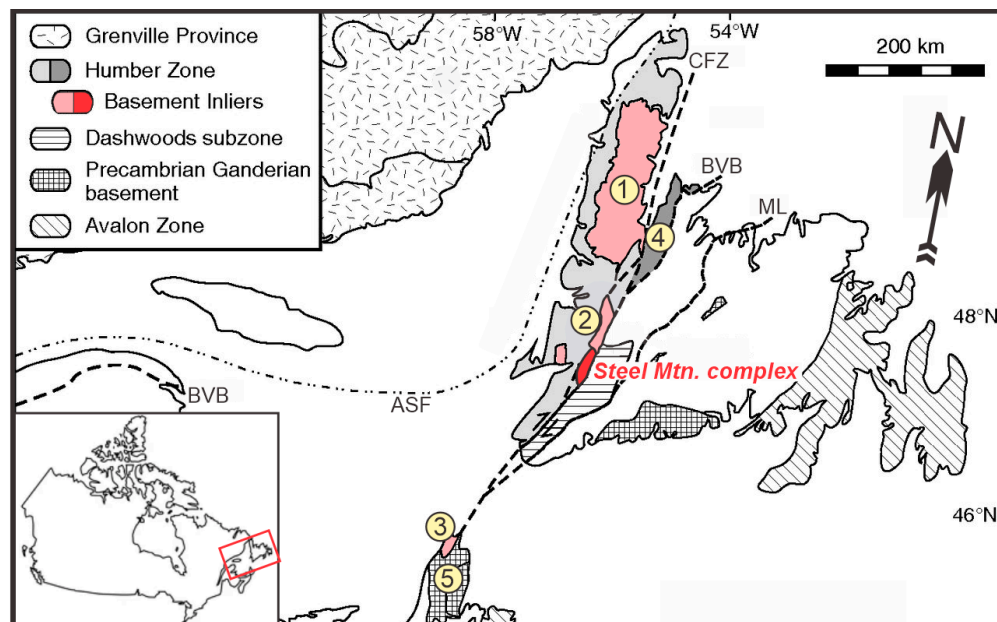


**Figure 1.** Regional map of the northern Appalachians showing the location of the Steel Mountain Anorthosite. Base map modified from [1]. ASF—Appalachian Structural Front; BVB—Baie Verte-Brompton Line; CFZ—Cabot Fault Zone; ML—Mekwe'jit Line (formerly Red Indian Line). (1)—Long Range Inlier; (2)—Corner Brook Lake block; (3)—Blair River Inlier; (4)—Fleur de Lys belt; (5)—Aspy and Bras d'Or terranes. (Original figure from Lin, S., Brem, A.G., van Staal, C.R., Davis, D.W., McNicoll, V.J., and Pehrsson, S., 2013, The Corner Brook Lake block in the Newfoundland Appalachians: A suspect terrane along the Laurentian margin and evidence for large-scale orogen-parallel motion: *GSA Bulletin*, v. 125, p. 1618–1632, <https://doi.org/10.1130/B30805.1>. Copyright© Geological Society of America. Used with permission).

## 2. Geological Setting

The Steel Mountain complex is one of a series of Proterozoic inliers along the north-western margin of the Appalachian Orogen in western Newfoundland and Cape Breton Island (Figure 1). It is tectonically juxtaposed with the Corner Brook Lake Block of Proterozoic and Silurian crystalline rocks [1]. U-Pb zircon dating of the Steel Mountain complex has yielded both 1.14 Ga and 0.6 Ga ages [2]. In the adjacent Corner Brook Lake Block, basement gneisses give U-Pb zircon ages of 1.5 Ga [1], and there are well-dated Ediacaran granitoid plutons [2]. The Steel Mountain complex is some 50 km long and consists principally of anorthosite and gabbronorite, previously mapped by van Berkel [11] and investigated mineralogically by Collins [12]. Diabase dykes with deformed margins cut the Steel Mountain anorthosite. The complex includes well-known magnetite deposits at the Bishop North and Bishop South localities [13]. In 1997, Loadstone Limited developed two quarries in the deposit (at 48.4026° N, 58.3319° W) for use as ballast in the Hibernia gravity-based offshore petroleum platform. In 1998, samples of this ore were transported to Moose River, Cumberland County, Nova Scotia, for possible use in the offshore petroleum industry on the Scotian Shelf. At that time, we acquired and studied these samples of the ore and its host rock [14].

### 3. Materials and Methods

Some 50 samples were examined, of which 15 were cut into polished thin sections for further investigation using a polarizing and reflected-light microscope, before performing analyses on selected mineral grains using the electron microprobe at the Regional Electron Microprobe Centre, Dalhousie University. These representative minerals were analyzed using a JEOL-733 machine with four wavelength spectrometers and a Tracor Northern 145-eV energy dispersive system detector. The beam operated at 15 kV and 15 nA and a beam diameter of 10  $\mu\text{m}$ . Geological standards were used. The data were reduced using a Tracor Northern ZAF matrix correction program.

Whole-rock geochemical analysis was carried out at Saint Mary's University on 13 samples using a Phillips PW2400 sequential X-ray fluorescence spectrometer (analytical details given in footnote to Table 1 of [15]). Sm/Nd isotopic analyses were performed at the University of Alberta using pulverized samples that were completely decomposed in a mixture of HF/HNO<sub>3</sub> acids. Sm and Nd were separated on cation-exchange columns, followed by separation on columns filled with BIORAD SX-1 bio-beads coated with DEP. 300–500 ng of Nd or Sm was loaded on a side of the Rhenium double filament bead and the isotopic composition was measured in a VG 354 mass spectrometer. Overall reproducibility of the isotopic measurements has been determined from a large number of measurements using the La Jolla Nd standard and the reproducibility of the concentration measurement has been determined from the Siberian Trap ST-2 local laboratory standard. At the 1% error level, the reproducibility for the <sup>143</sup>Nd/<sup>144</sup>Nd and <sup>147</sup>Sm/<sup>144</sup>Nd are 0.001% to 0.002% and 0.3% to 0.5%, respectively. The <sup>143</sup>Nd/<sup>144</sup>Nd ratios of the analyzed samples have been normalized to the La Jolla standard value of 0.511858. Handpicked biotite grains were dated by the <sup>40</sup>Ar/<sup>39</sup>Ar method using laser step-heating at the Queen's University geochronology lab using methods outlined by [16].

### 4. Petrography

Three main rock types are present: anorthosite, gabbro-norite, and magnetite-ilmenite ore. Both anorthosite and gabbro-norite occur as cumulate and non-cumulate rocks and some contain megacrysts of plagioclase, pyroxene, and amphibole up to 5 cm in length. Many samples are deformed with granulation textures. The ores are principally magnetite and ilmenite in veins and blobs with lobate contact relationships with anorthosite.

#### 4.1. Anorthosite

Fresh anorthosite is dark gray or pinkish-gray. All samples contain plagioclase in excess of 90% of the total volume. Some samples contain larger plagioclase laths forming adcumulate to mesocumulate textures with smaller intercumulate plagioclase crystals. Other samples show non-cumulate textures. Some samples show granulation, much of which appears to be autoclastic prior to full crystallization. The anorthosite also shows varying tectonic deformation, with flattening deformation, folding, and shearing (Figure 2c).

The cumulate plagioclase megacrysts of andesine composition range in length from 1 to 5 cm (Figure 2d). These crystals are subhedral where their overgrowths have crystallized from intercumulate liquid. An adcumulate texture is produced where the cumulate plagioclase crystals and their overgrowths are the only components of the texture. In the non-cumulate anorthosite, the plagioclase forms allotriomorphic-granular textures, as the result of in situ crystallization. These rocks show little variation in crystal size (1–2 cm), shape, or composition (andesine).

In some anorthosites, large plagioclase megacrysts contain abundant mineral inclusions, either as independent crystals or in clusters of up to about 20 crystals. The widespread independent crystals are dominantly amphibole, magnetite, biotite, epidote, K-feldspar, and titanite (Figure 3d). The dominant mineral in the clusters is plagioclase with lesser amphibole and biotite as smaller euhedral crystals. The mineral clusters are interpreted as cognate inclusions that were trapped during the crystallization of the megacryst.

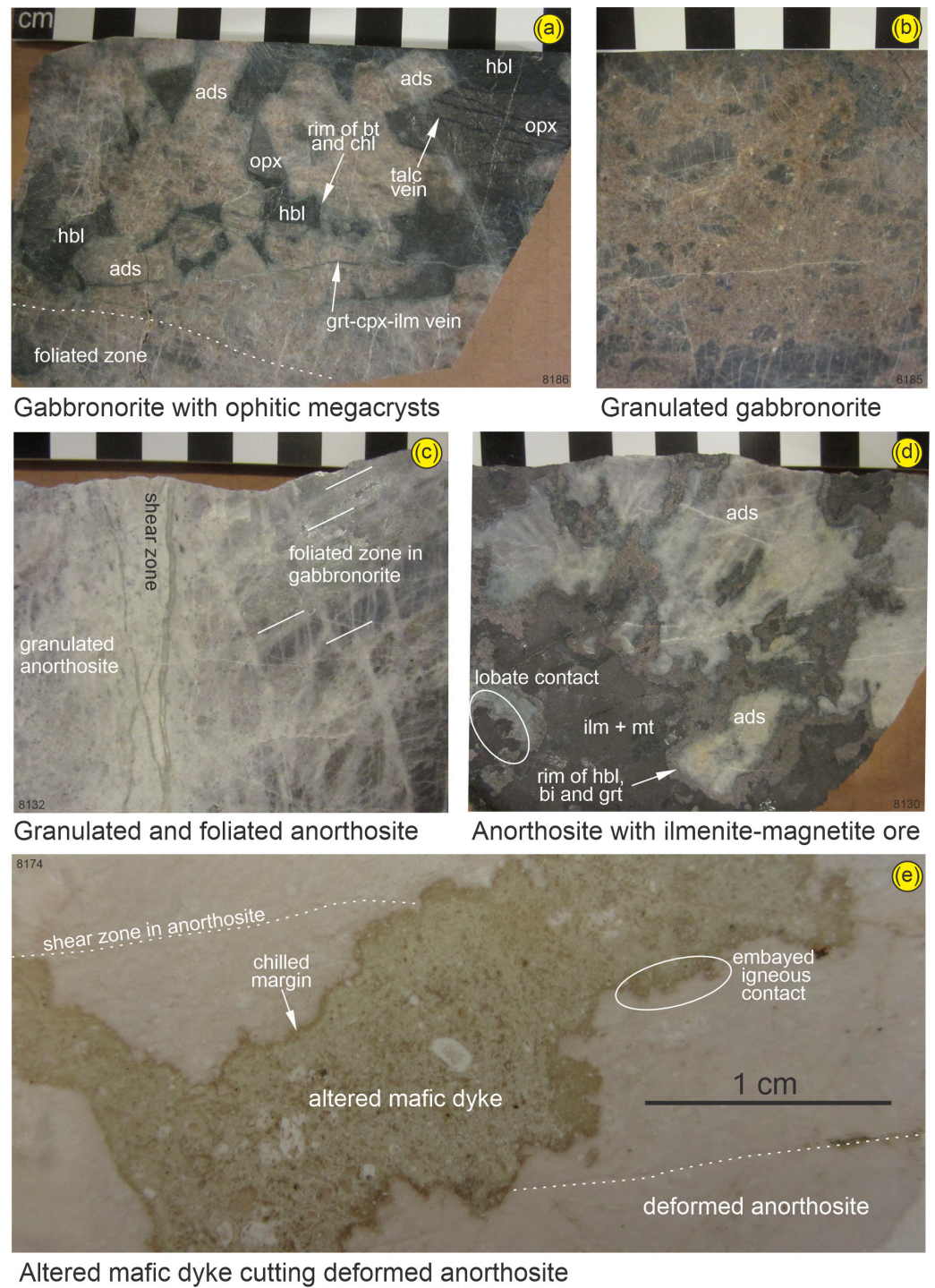


**Figure 2.** Photographs of rock slabs showing textural relationships of minerals in gabbrorite and anorthosite. (a) Ophitic texture of ferromagnesian minerals and andesine plagioclase. Arrows point to small features. (b) Autoclastic granulated gabbrorite; dark minerals are orthopyroxene and hornblende. (c) Granulated and foliated anorthosite. Foliation indicated by short lines. (d) Mix of Fe-Ti oxide rock with anorthosite, showing lobate contacts with corona rims of hornblende, biotite, and garnet. (e) Thin section of altered mafic dyke with a chilled margin cutting tectonically deformed anorthosite. In this and subsequent figures, IMA abbreviations [17] are used, including: ads—andesine; bt—biotite; chl—chlorite; cpx—clinopyroxene; hbl—hornblende; grt—garnet; ilm—ilmenite; mt—magnetite; opx—orthopyroxene.

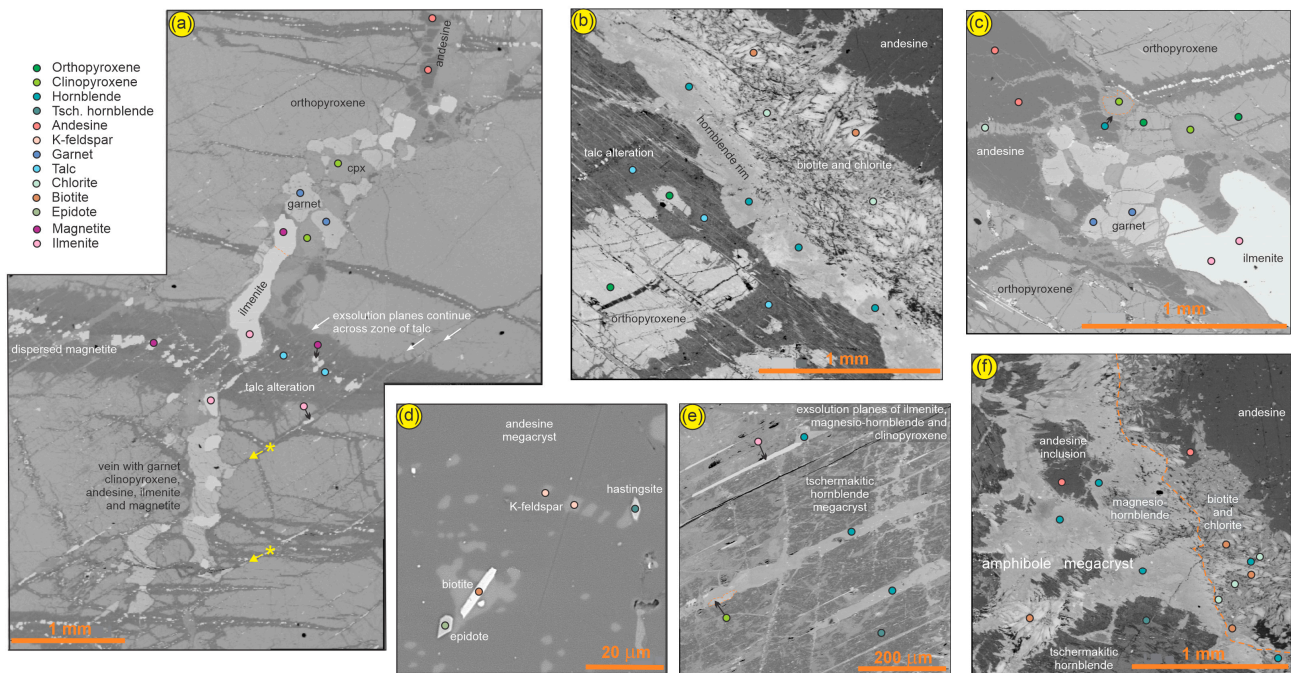


**Figure 3.** Backscattered electron (BSE) images of textural relationships of minerals in gabbronorite and anorthosite. Colored dots indicate EDS mineral analyses. (a) Gabbronorite cut by discontinuous vein with garnet, clinopyroxene, andesine, ilmenite, and magnetite, in turn, cut by an alteration zone of talc and dispersed magnetite across which some exsolution lamellae continue. \*→ indicates where veins have invaded exsolution lamellae. (b) Gabbronorite with orthopyroxene megacrysts patchily altered to talc, with a rim of hornblende, biotite, and chlorite in contact with andesine megacrysts. (c) Gabbronorite with vein of ilmenite, garnet, hornblende, and clinopyroxene. (d) Anorthosite showing inclusions in andesine megacrysts. (e) Tschermakitic hornblende megacrysts with exsolution lamellae of ilmenite, Magnesio-hornblende, and clinopyroxene. (f) Gabbronorite with megacrystic amphibole showing tschermakitic- and Magnesio-hornblende phases and a rim of biotite and chlorite in contact with andesine megacrysts.

Anorthosite forms lobate contacts with magnetite-ilmenite ores, with a well-developed rim or corona of hornblende, biotite, and garnet (Figure 2d). One anorthosite sample is cut by a centimeter-wide altered mafic dyke (Figure 2e). The dyke consists largely of albite, epidote, titanite, and calcite, with common euhedral zircon crystals (Supplementary Table S1; Supplementary Figure S1). The dyke has a finer-grained chilled margin against the anorthosite and shows invasive igneous contacts that cross-cut brittle deformation in the anorthosite. Except for this sample, we were unable to locate zircon grains in our thin sections from the anorthosite and gabbronorite samples.

#### 4.2. Gabbronorite

Gabbronorite samples are typically pinkish-gray. Plagioclase is the dominant mineral (Figure 2a), generally with a modal abundance of >60%, showing gradation through leucogabbronorite to anorthosite. All ferromagnesian and opaque minerals are postcumulus phases, and along with plagioclase, occur as intercumulate crystals between large laths of cumulate plagioclase, producing the dominantly mesocumulate textures of these rocks. Some gabbronorite samples show centimeter-scale rhythmic layering between plagioclase laths and elongated bands of the ferromagnesian minerals, which is likely due to pre-full crystallization tectonic deformation. Some samples show autoclastic granulation (Figure 2b). Orthopyroxene, Mg-rich hypersthene, makes up >65% of the ferromagnesian minerals and typically forms smallish (<1 cm) euhedral crystals. Minor clinopyroxene (diopside) occurs as small (<1 mm) euhedral crystals, in contact with the orthopyroxene (Figure 3a). Magnesio-hornblende occurs as a thin overgrowth around orthopyroxene (Figure 3b).

#### 4.2.1. Megacrystic Gabbronorite

Orthopyroxene (Figure 3a) and amphibole (Figure 3e,f) are the two most abundant megacrystic minerals in some gabbronorite samples, ranging in size from 1 to >10 cm (Figure 2a). Most ferromagnesian megacrysts occur within a groundmass of small plagioclase crystals surrounded by several large euhedral plagioclase megacrysts, which control the shape of the ferromagnesian megacrysts, and form subophitic–ophitic textures (Figure 2a). Contacts between amphibole and orthopyroxene are sharp, preserving the original igneous texture.

The orthopyroxene megacrysts are highly fractured with two distinct sets of fractures with ambiguous cross-cutting relationships (Figure 3a). (1) A set of fractures is filled with veins of small crystals of clinopyroxene, garnet, ilmenite, magnetite, and plagioclase where they cross the orthopyroxene megacrysts. (2) A sub-parallel set of fractures orthogonal to these multi-mineralic veins is the site where talc has replaced orthopyroxene and the center of these fractures hosts strings of dispersed magnetite crystals. Talc also replaces orthopyroxene at the margins of some megacrysts (Figure 3b). Although the multi-mineralic veins appear to cut the talc alteration zones, if the talc forms only from an orthopyroxene precursor, then the multi-mineralic veins may have formed earlier (note the gap in the vein in Figure 3a). The amphibole megacrysts show a patchy texture of areas with more tschermakitic hornblende (darker on the BSE images) and more actinolitic hornblende (lighter on the BSE images) (Figure 3e,f).

Megacrysts of both amphibole and orthopyroxene show corona structures. The rims consist of an inner layer of microcrystalline magnesio–hornblende around both orthopyroxene (Figure 3b) and amphibole megacrysts (Figure 3f). In both cases, there is also an outer layer of finely crystalline biotite, which in some places has altered to chlorite.

The orthopyroxene and amphibole megacrysts contain abundant discontinuous exsolution lamellae, parallel to their cleavage planes, consisting of iron–titanium oxides, amphibole, and clinopyroxene (Figure 3a,e). The oxide lamellae are most abundant and consist dominantly of hemo-ilmenite or ilmenite. Clinopyroxene occurs only as small domains within amphibole lamellae (Figure 3e). The lamellae extend through the talc alteration zones but terminate at the multi-mineralic veins (Figure 3a).

#### 4.2.2. Gabbronorite with Mafic Layering

Layers enriched in ferromagnesian minerals are common in the Steel Mountain gabbronorite. Large euhedral crystals of orthopyroxene and hornblende have crystallized, along with plagioclase megacrysts, as cumulate crystals. Smaller groundmass crystals are interpreted as intercumulate minerals that crystallized along with plagioclase during the final stages of crystallization of an intercumulate liquid. The most common ferromagnesian intercumulate minerals are orthopyroxene and clinopyroxene. These generally equant grains form ophitic to sub-ophitic textures with the plagioclase laths. Other intercumulate minerals include biotite, which commonly occurs associated with or rimming magnetite or ilmenite. Pyrite is present in minor amounts as an intercumulate mineral associated with minor amounts of chalcopyrite and pentlandite. The clinopyroxene and orthopyroxene are partly altered to chlorite in some samples.

Primary magnesio–hornblende occurs as an intercumulate mineral in some samples, with minor amounts of orthopyroxene (dominantly as relict crystals) and clinopyroxene, biotite, and magnetite. The amphibole shows the same equant, ophitic to sub-ophitic, textures as the intercumulate orthopyroxene and clinopyroxene. Some amphibole crystals have been almost completely altered to minerals tentatively identified from chemistry as smectite or chlorite. The layered rocks are cut by several sub-parallel fractures, similar to those observed cutting the megacrystic gabbronorite, which preferentially cut the mafic layers. Chlorite fills the fractures that cut plagioclase, while talc ± magnetite fills fractures that cut the ferromagnesian minerals.

### 4.3. Magnetite-Ilmenite Ore

The magnetite-ilmenite ore rocks consist principally of coarse-grained magnetite and ilmenite (Figure 4), with <10% plagioclase and orthopyroxene crystals, which are most common near contacts with silicate rocks. Other silicate inclusions comprise pargasite, spinel (Mg-rich hercynite) that have been partially altered to corundum (Figure 4a), and almandine-rich (Alm<sub>66</sub>–Alm<sub>81</sub>) euhedral garnet crystals (Figure 3c). Olivine crystals are altered to antigorite (Figure 4b). Crystals of iddingsite, presumably after olivine, are also replaced by antigorite (Figure 4c). Various iron sulfide minerals, principally pyrrhotite, with some pentlandite and chalcopyrite, are also present (Figure 4a,b).

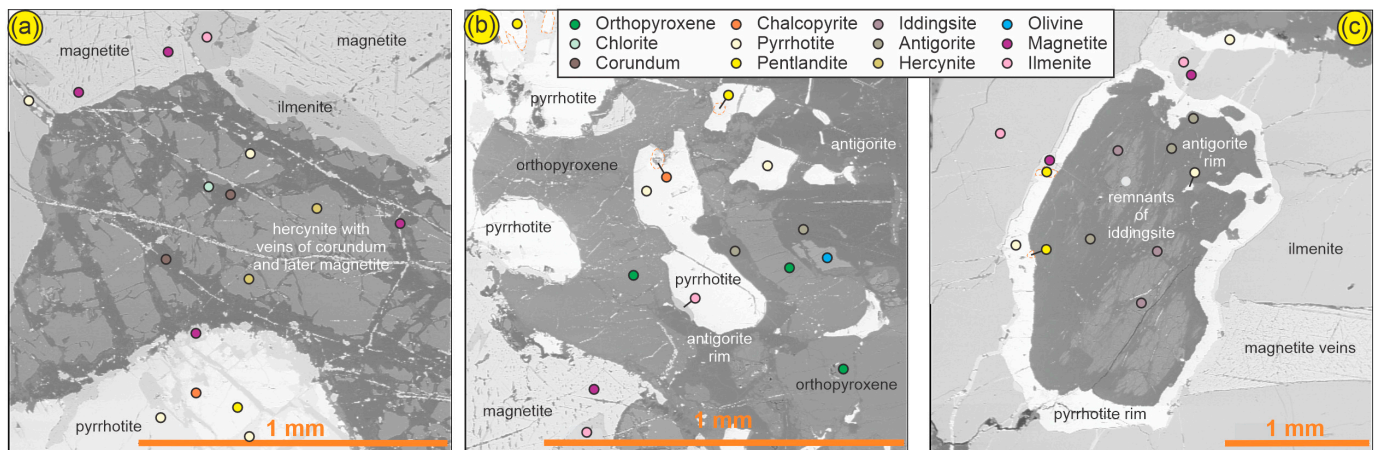


**Figure 4.** Backscattered electron images of textural relationships of silicate minerals in magnetite-ilmenite ore. (a) Inclusion of hercynite. (b) Irregular inclusion of orthopyroxene and olivine altered to antigorite. (c) Iddingsite after olivine, largely altered to antigorite and rimmed by pyrrhotite.

## 5. Mineral Chemistry

### 5.1. Feldspar

The plagioclase crystals are unzoned and have compositions from An<sub>31</sub> to An<sub>49</sub> (Figure 5). Plagioclase in gabbronorite is slightly more anorthitic (mostly An<sub>46–47</sub>) than that in anorthosite (mostly An<sub>43–45</sub>). Plagioclase megacrysts mixed in magnetite-ilmenite ore are distinctly more albitic (An<sub>31–32</sub>).

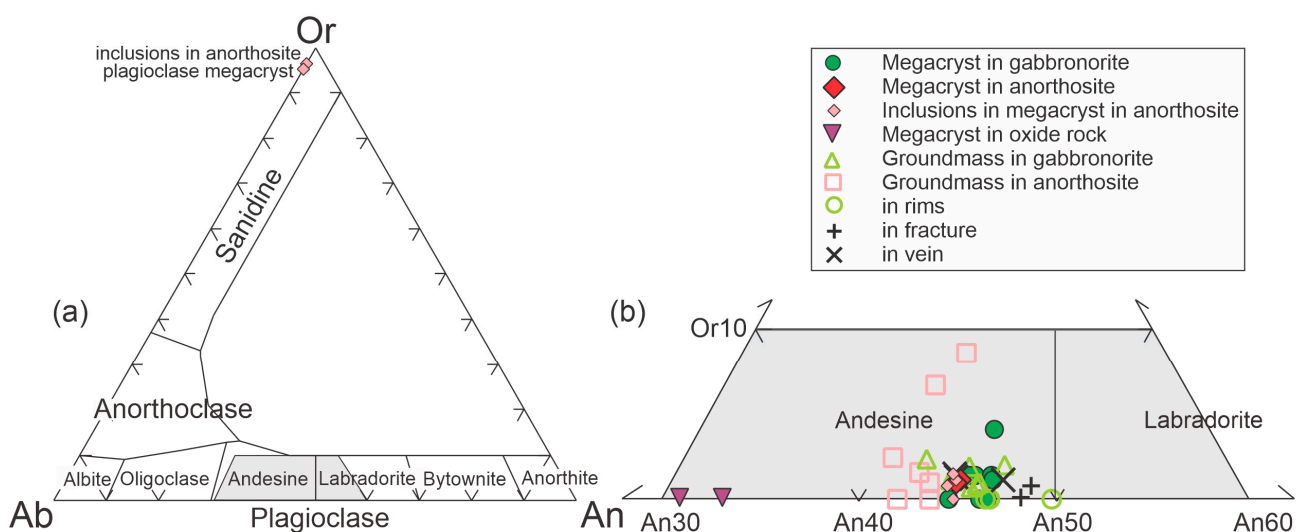


**Figure 5.** Composition of feldspars. (a) Ternary Or-Ab-An plot (after [18]) showing K-feldspar compositions. All plagioclase plots are in the grey field. (b) Detail of plagioclase compositions. Ab—albite, An—anorthite, Or—orthoclase.

### 5.2. Orthopyroxene

The groundmass orthopyroxene varies from En<sub>62</sub>–En<sub>67</sub> and the orthopyroxene megacrysts from En<sub>67</sub>–En<sub>70</sub>. The spot analyses of the megacrysts (En > 67%) are typically more Mg-rich compared to the groundmass orthopyroxene (En < 67%) (Figure 6) and show some variations in minor elements such as Al<sub>2</sub>O<sub>3</sub>, MnO, CaO, and TiO<sub>2</sub>. The variations in minor elements within the megacrysts generally overlap the variations in groundmass orthopyroxene compositions. The similarity of minor elements between the spot analyses of the megacrysts and the groundmass orthopyroxene provides a link to a similar local environment. This is supported by the lack of any zoning in the megacrysts.

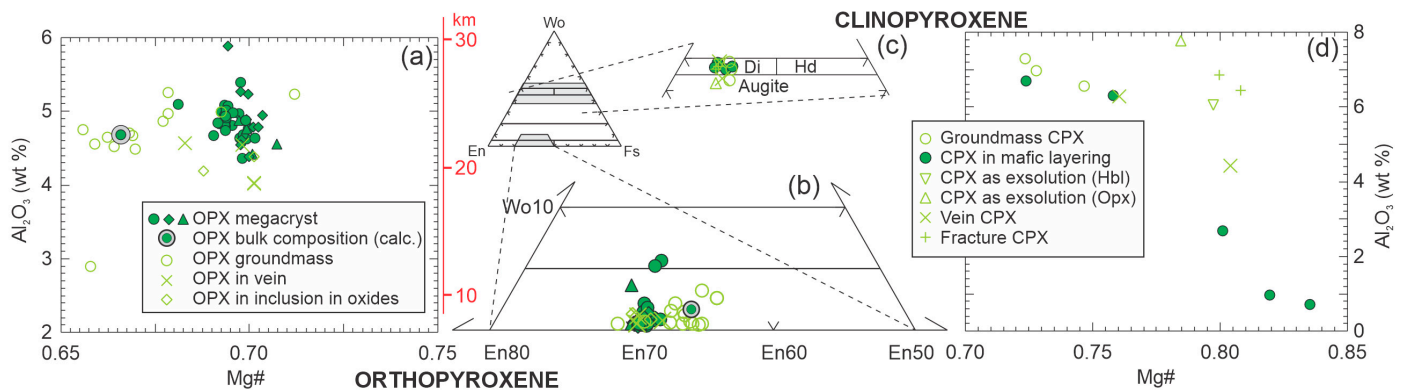


**Figure 6.** Chemical composition of pyroxenes, nomenclature of [18]. (a) Al content and Mg# of orthopyroxene (opx). Depth of crystallization (in red) from [6]. (b,c) En-Fs-Wo ternary plot of ortho- and clinopyroxenes (cpx) (respectively). (d) Al content and Mg# of clinopyroxene. Di—diopside, En—enstatite, Fs—ferrosilite, Hd—hedenbergite, Wo—wollastonite.

The spot analyses are not representative of the composition of the orthopyroxene as it was when it crystallized, since hemo-ilmenite, amphibole, clinopyroxene, and probably ilmenite have been exsolved. The original bulk composition of the orthopyroxene must therefore include the elements in these minerals. A recalculation of the bulk composition of the megacrystic orthopyroxene based on modal abundances of 5% hemo-ilmenite, 2% amphibole (magnesian-hornblende), and 1% clinopyroxene yields a composition of En<sub>65</sub>Fs<sub>33</sub>Wo<sub>2</sub>. The bulk composition of the megacrystic orthopyroxene is enriched in iron (Fs<sub>33</sub>) compared to the spot analyses and very similar to the groundmass orthopyroxene (Figure 6b). The bulk composition is also enriched in TiO<sub>2</sub> (1.94 wt%) and MnO (0.30 wt%). The Mg# values generally decrease from the bulk orthopyroxene to groundmass orthopyroxene and increase to the spot analyses of the megacrysts (Figure 6a). The iron-rich bulk composition of the megacrysts compares very well with the groundmass orthopyroxene and suggests that the megacrysts did not form during a much earlier stage of crystallization, but rather contemporaneously from a similar Fe-rich magma.

### 5.3. Clinopyroxene

Clinopyroxene is not a common mineral in these rocks and it occurs only in small amounts as a groundmass mineral in the gabbro-norites, as an exsolution mineral in the megacrysts, and in veins and fractures. Clinopyroxene crystals in mafic layers are generally diopside, with a composition around Wo<sub>46.6</sub>En<sub>38.8</sub>Fs<sub>14.6</sub> (Figure 6d). Exsolution lamellae of clinopyroxene in orthopyroxene are of augite composition (~Wo<sub>44</sub>En<sub>44</sub>Fs<sub>12</sub>).

### 5.4. Amphibole

Amphibole megacrysts consist of somewhat tschermakitic magnesian-hornblende (Figure 7). The megacrysts have exsolved ilmenite, magnesian-hornblende, clinopyroxene, and titanite. Most amphiboles analyzed from inclusions in plagioclase, both in individual crystals and in clusters of crystals, are hastingsite or, less commonly, pargasite. Applica-

tion of the Al-in-hornblende geobarometer [19] suggests that the inclusions in plagioclase formed at 0.7–1.0 GPa and the megacrysts at 0.4–0.6 GPa. Exsolution lamellae in orthopyroxene and tschermakitic hornblende are of magnesio–hornblende composition.

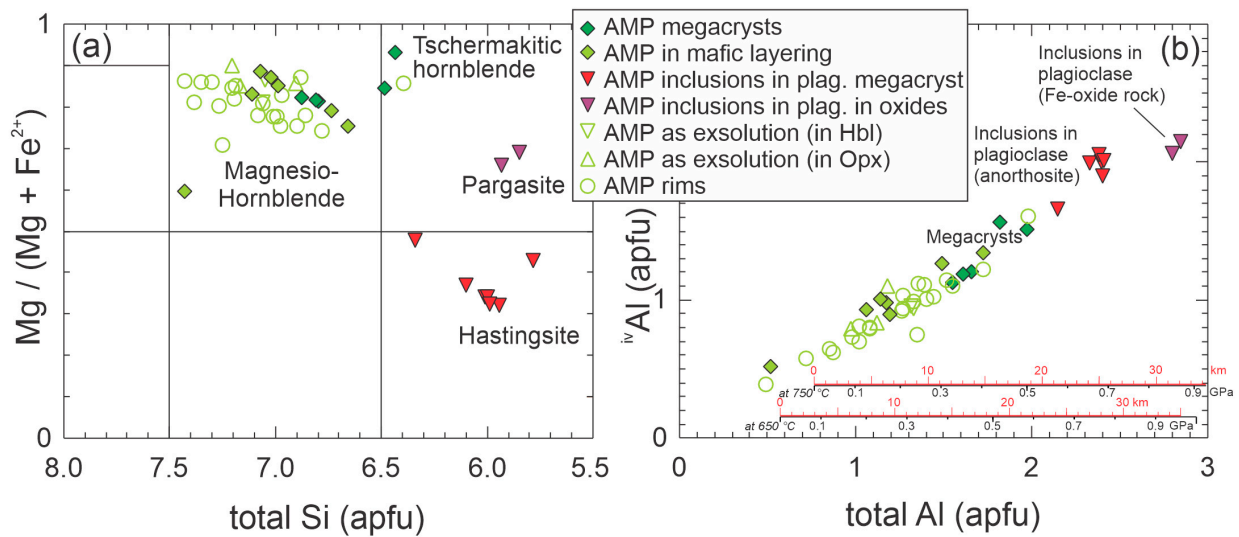


**Figure 7.** Chemical composition of amphibole. (a) Plot of Mg/(Mg + Fe<sup>2+</sup>) vs. Si showing nomenclature of principal amphibole types [20]. (b) Plot of <sup>iv</sup>Al vs. total Al showing geobarometric estimates for temperatures of 650° and 750 °C [19].

### 6. Lithochemistry

Whole-rock geochemical analysis was carried out on nine anorthosites and seven gabbronorites. Representative analyses are shown in Table 1 and trace element variation is illustrated in Figure 8. The chemistry of both rock types is dominated by the abundance of plagioclase. Trace elements also reflect the chemistry of plagioclase (relatively high Sr and Eu) and the presence of minor K-feldspar (high Rb, Ba, and K). Low Nb appears to be a primary feature of the magma, rather than a result of scavenging by an immiscible oxide magma, as the anorthosite 8157 with oxide inclusions has low Nb, despite high Ti (Figure 8) and >6.5 wt.% Fe<sub>2</sub>O<sub>3</sub> (Table 1).

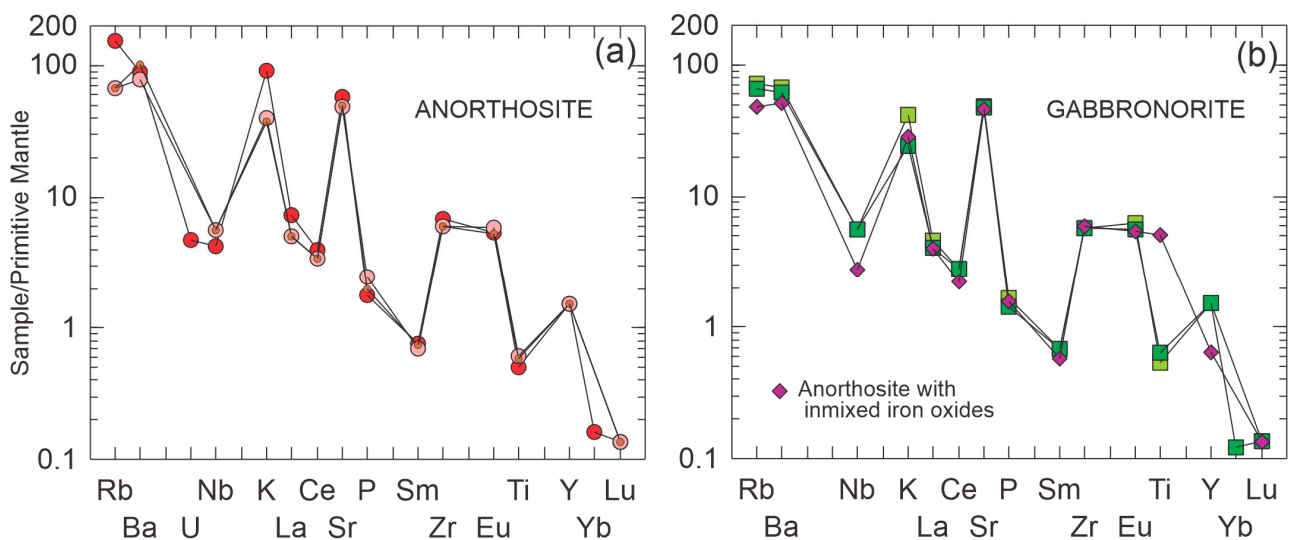


**Figure 8.** Trace element composition of (a) anorthosite and (b) gabbronorite and anorthosite with inmixed iron oxides. Normalizing factors from [21] were used.

**Table 1.** Whole-rock analyses of anorthosite (an) and gabbronorite (gn).

Rock Type	an	an	an	an	an +	gn	gn	gn	gn
Sample	8127	8128	8150	8154	8157	8129	8153	8185	8187
Major oxides (wt%)									
SiO <sub>2</sub>	56.09	54.85	55.3	55.47	51.19	54.90	54.45	55.75	53.20
TiO <sub>2</sub>	0.13	0.38	0.13	0.12	1.10	0.18	0.12	0.14	0.32
Al <sub>2</sub> O <sub>3</sub>	26.88	27.49	27.04	26.49	25.01	25.62	25.98	26.92	21.08
Fe <sub>2</sub> O <sub>3t</sub>	1.26	2.32	0.61	0.58	6.65	2.30	0.64	1.28	6.83
MnO	0.02	0.02	0.01	0.00	0.03	0.03	0.01	0.02	0.11
MgO	0.44	0.32	0.19	0.19	0.62	2.04	0.15	0.95	7.13
CaO	8.21	8.84	8.14	8.18	7.55	8.21	8.53	8.61	6.85
Na <sub>2</sub> O	5.67	5.43	5.87	5.67	5.19	5.32	5.63	5.5	3.73
K <sub>2</sub> O	1.12	0.86	1.18	1.04	0.85	0.69	1.21	0.75	0.53
P <sub>2</sub> O <sub>5</sub>	0.04	0.03	0.04	0.03	0.03	0.03	0.04	0.03	0.03
L.O.I.	0.60	0.49	0.20	0.84	0.70	1.01	1.83	0.76	0.61
Total	100.46	101.03	98.71	98.61	98.92	100.33	98.59	100.71	100.42
Trace elements (ppm)									
Ba	713	515	483	229	359	261	467	432	302
Rb	43	40	47	47	31	40	46	42	29
Sr	1044	1007	1091	1023	984	923	1024	996	696
Y	7	4	8	6	3	7	7	7	6
Zr	67	65	70	64	67	61	64	64	57
Nb	4	3	4	4	2	3	4	4	3
Th	1	2	2	3	b.d.	b.d.	2	b.d.	b.d.
Pb	5	4	8	7	4	6	7	7	2
Ga	23	22	23	24	19	22	23	23	18
Zn	b.d.	14	b.d.	b.d.	39	19	b.d.	4	61
Cu	20	8	9	11	47	7	8	6	4
Ni	49	27	24	26	104	33	21	24	65
V	26	51	12	b.d.	193	32	10	b.d.	75
Cr	8	27	10	7	108	23	8	19	114
Co	b.d.	b.d.	b.d.	b.d.	22	4	b.d.	b.d.	34
Sc	b.d.	b.d.	4	3	b.d.	b.d.	b.d.	b.d.	6
La	19	13	17	14	12	15	12	22	15
Ce	61	b.d.	18	52	32	b.d.	37	b.d.	21
Nd	15	11	9	7	13	5	8	14	10

+ sample with Fe-Ti oxide inclusions in anorthosite; b.d.—below detection limit.

Two bulk samples of anorthosite and two of gabbronorite were analyzed for Nd/Sm isotopes (Table 2). The samples define an apparent isochron of  $1.2 \pm 0.2$  Ga (Figure 9a) and have an average depleted-mantle-model age of 1.38 Ga.  $\epsilon_{Nd}$  was calculated for three possible emplacement ages of the rocks: 0.6 Ga (based on [2]), 1.2 Ga (our isochron), and 1.5 Ga (based on [1]) (Table 2; Figure 9b). The strongly negative values of  $\epsilon_{Nd}$  at 0.6 Ga are quite unlike any Proterozoic anorthosites in the literature (Figure 14 of [4]) and the values

at 1.5 Ga are similar only to unusually high values found in the literature. In contrast, the  $\epsilon_{Nd}$  values at 1.2 Ga are close to the median Proterozoic value in the literature.

**Table 2.** Nd-Sm isotopes for anorthosite and gabbronorite.

Sample	Lithology	Measured				Calculated			
		Sm ppm	Nd ppm	$^{147}\text{Sm}/^{144}\text{Nd}$	$^{143}\text{Nd}/^{144}\text{Nd}$	$t_{DM}$ (Ga)	$\epsilon_{0.6\text{ CHUR}}$	$\epsilon_{1.2\text{ CHUR}}$	$\epsilon_{1.5\text{ CHUR}}$
8217	anorthosite	0.29	2.21	0.0802	0.511856	1.35	−6.33	2.66	7.18
8131A	anorthosite	0.25	1.84	0.0825	0.511839	1.39	−6.84	1.97	6.40
8131B	gabbronorite	0.32	2.27	0.0848	0.511869	1.38	−6.43	2.20	6.54
8187	gabbronorite	0.3	1.77	0.1013	0.512006	1.40	−5.02	2.34	6.04

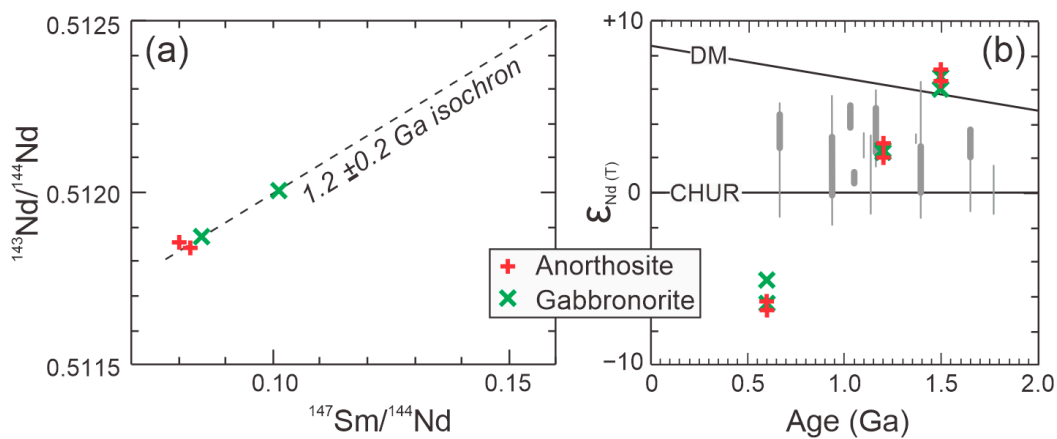


**Figure 9.** (a)  $^{143}\text{Nd}/^{144}\text{Nd}$  vs.  $^{147}\text{Sm}/^{144}\text{Nd}$  showing inferred Mesoproterozoic isochron. (b) Plot of  $\epsilon_{Nd}$  vs. age for three possible ages of the Steel Mountain anorthosite. Grey bars are values for other Proterozoic anorthosites from [4].

### 7. Geochronology

The dated biotite grains were from the altered rim of an amphibole-bearing anorthosite. The conventional  $^{40}\text{Ar}/^{39}\text{Ar}$  age spectrum (Figure 10) shows a monotonic age increase from an initial low temperature step at 290 Ma (Permian) to a plateau age of  $485 \pm 4$  Ma ( $2\sigma$ ) (Early Ordovician). The final heating step of the sample defines an age of 776 Ma (Cryogenian), which, based on the Ca/K ratio, is likely to be from an amphibole component.

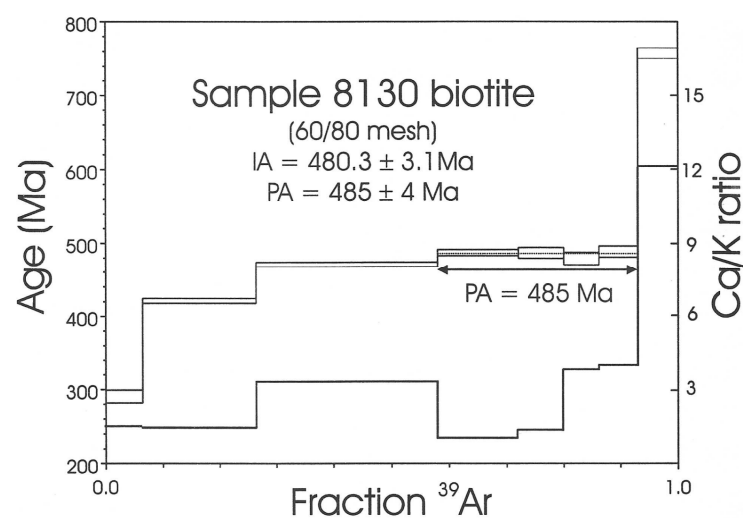


**Figure 10.**  $^{40}\text{Ar}/^{39}\text{Ar}$  age spectrum for biotite rimming amphibole in anorthosite. Data in Supplementary Table S2.

## 8. Discussion

### 8.1. Magmatic Crystallization

Based on textural relationships, the megacrystic plagioclase crystals were the first to crystallize. The ferromagnesian megacrysts crystallized contemporaneously or immediately following the plagioclase megacrysts, as suggested by the subophitic–ophitic textures, with orthopyroxene crystallizing earlier than amphibole (Figure 2a).

The Al-in-orthopyroxene geobarometer [5,6] indicates a crystallization depth of 22–25 km for orthopyroxene megacrysts. Groundmass orthopyroxene is of similar composition and its Mg# is similar to that for the megacrysts after correction for exsolution (Figure 6). Rare orthopyroxene in the ilmenite–garnet–clinopyroxene veins is a little less aluminous, suggesting a crystallization depth of 19–21 km. The Al-in-hornblende geobarometer [19] is temperature dependent and thus difficult to compare directly with the orthopyroxene. The highest pressure amphiboles occur as inclusions in andesine megacrysts (Figure 7b) and suggest crystallization at depths of 30–35 km. Estimates for amphibole megacrysts are 15–20 km and for amphibole in layered gabbro-norite 10–18 km.

Thus, mineral textures and chemistry provide evidence of polybaric crystallization of the massif anorthosite, similar to that found by [6]. A buoyant plagioclase crystal mush [4] accumulated over depths of 35–22 km and gradually rose through the magmatic plumbing system [22], with the crystallization of gabbro-norite orthopyroxene at 22–25 km as both megacrysts and groundmass are of similar composition. The formation of megacrysts was likely due to Ostwald ripening [23], when crystals precipitate from magma at high temperatures close to their liquidus, so that large crystals grow at the expense of smaller crystals. Minor deformation of the rising mush allowed the emplacement of the ilmenite–garnet–clinopyroxene veins. As the anorthositic mush rose higher through the crust, the ambient magma became more hydrous, favoring the crystallization of amphibole megacrysts (Figure 2a).

Primary coarse-grained igneous amphibole is known from Archean anorthosites [4,24], although much appears to be of metamorphic origin. In Proterozoic anorthositic massifs, amphibole is very rare and is found mostly as inclusions. For example, considering other anorthosite massifs in southeastern Canada, the Labrieville anorthosite, Quebec, has hornblende either in an inclusion-like form together with plagioclase within pyroxene megacrysts or together with biotite at megacryst margins [7]. The Lac Chaudière anorthosite, Quebec, has small amounts of hornblende in each orthopyroxene megacryst, as small flakes at the megacryst margins, and as thin plates within plagioclase exsolution lamellae [8]. Ferroan-pargasitic-hornblende subhedra occur in a few samples in the Chateau-Richer anorthosite, Quebec [10]. The Nain anorthositic complex has small amounts of amphibole in orthopyroxene megacrysts [9]. The abundance of amphibole in the Steel Mountain anorthosite massif is much greater than in typical Proterozoic anorthosite massifs. This is not solely the effect of shallow crystallization depths, as comparable depths are recorded in other anorthosite massifs [6]. Rather, it suggests greater overall availability of water in the parent magma.

Massive magnetite-ilmenite ores have been reported in association with many anorthosite massifs (e.g., [7,9]). The deposits may be concordant or discordant, having been produced through the injection or accumulation of immiscible Fe-Ti-rich liquid [25]. The lobate contacts against anorthosite in the studied samples suggest an origin from an immiscible magma in a crystal mush. Both olivine and iddingsite are present (Figure 4b,c), and the highest pressure amphiboles found in this study are in plagioclase inclusions in magnetite-ilmenite ore.

The altered cm-wide mafic dyke with common zircon (Figure 2e) cross-cuts shear zones in anorthosite and is thus a later igneous event of unknown age. Whether it is related to mafic dykes reported as cutting the Steel Mountain complex [11] is unknown.

### 8.2. Sub-Solidus Alteration

The exsolution of ilmenite in ferromagnesian megacrysts (Figure 3a,e,f) appears earlier than the fracturing and vein filling by ilmenite, garnet and clinopyroxene (\*→ in

Figure 3a). Both of these events appear to predate pervasive fracturing and hydration of orthopyroxene to talc and granular magnetite (Figure 3a,b). The relative timing of other sub-solidus alteration is unclear. There was patchy alteration of tschermakitic hornblende to magnesio-hornblende (Figure 3e,f) similar to that described by [26]. Corona rims of magnesio-hornblende, biotite, and chlorite formed around the orthopyroxene and amphibole megacrysts (Figure 3b,f).

The exsolution minerals in the orthopyroxene megacrysts of the Steel Mountain anorthosite and gabbro-norite consist of hemo-ilmenite, magnesio-hornblende, and clinopyroxene. This assemblage of exsolution minerals appears unique to the Steel Mountain complex. The most common exsolution mineral in orthopyroxene megacrysts from other massif anorthosites is plagioclase, which is commonly associated with clinopyroxene, Fe-Ti oxides, garnet, and minor biotite [5,27]. The suppression of plagioclase exsolution at Steel Mountain was probably due to high water content [28], which also favored the precipitation of amphibole and the alteration of orthopyroxene to talc. The source of Ti to form the ilmenite exsolution lamellae is unclear. About 8% of EMPA analyses of orthopyroxene, both megacrysts and groundmass, have measurable Ti ranging from 0.2%–0.4% Ti [14] and the bulk-rock Ti content of gabbro-norite is 0.12% Ti (Table 1), mostly in ilmenite with less in clinopyroxene and amphibole. Most of the analyzed megacrysts have exsolution lamellae of ilmenite and may thus have already lost Ti.

Sub-solidus alteration in the ilmenite-magnetite ore includes the alteration of olivine to iddingsite and then antigorite (Figure 4b,c) and the alteration of hercynite to corundum and later magnetite veins (Figure 4a).

### 8.3. Age and Tectonic Affinity of the Steel Mountain Complex

The ~290 Ma initial heating step in the Ar-Ar spectrum of the biotite (Figure 10) is probably the result of high heat flow in the Deer Lake Basin in the early Carboniferous period [29], followed by uplift and unroofing by the early Permian period, as recorded in apatite fission track studies [30]. The main early Ordovician plateau age of the biotite is synchronous with the Taconic 2 continental arc magmatism on the Laurentian margin of the Appalachians and the Penobscot subduction on the peri-Gondwanan Gander terrane [31]. There is no thermal record of the widespread mid-Silurian magmatism of the Corner Brook Lake Block [1]. The late Tonian ~780 Ma final heating step is broadly synchronous with the oldest igneous activity in the peri-Gondwanan Avalon terrane [32].

The estimated 1.2 Ga age for emplacement of the Steel Mountain anorthosite (Figure 9) would be consistent with a peri-Gondwanan origin from the southern Appalachians, with the 1.2 Ga age and Nd-Sm isotopes similar to inferred basement contributions to the Hyco arc volcanic rocks of North Carolina [33]. In contrast, detrital zircons of Laurentian origin generally show major peaks at 1.0 and 1.5 Ga [34]. Although the Steel Mountain complex probably has a peri-Gondwanan origin from the southwestern US Appalachians, its assembly with the peri-Gondwanan Corner Brook Lake Block probably post-dates the voluminous Ediacaran magmatism in that Block.

The host rock of the 0.6 Ga zircons dated by [2] is reported only as Steel Mountain anorthosite and was collected 20 km NE of our outcrops. Their zircon ages appear inconsistent with our Nd-Sm ages and with the lack of zircon in the anorthosite and gabbro-norite samples that we examined in detail. The only zircon grains that we found in our study are in the late mafic dyke that has been highly altered to albite, epidote and titanite (Figure 2e).

## 9. Conclusions

1. The Steel Mountain complex is a typical Proterozoic anorthosite massif, except for the abundance of amphibole, which indicates more hydrous magmatic conditions than in Laurentian anorthosites in the literature.
2. The ferromagnesian megacrysts have exsolution lamellae of Fe-Ti oxides, magnesio-hornblende, and clinopyroxene. The lack of exsolution lamellae of plagioclase is

- unusual for Proterozoic anorthosites and is a consequence of hydrous conditions in the Steel Mountain anorthosite.
3. Sub-solidus exsolution of ilmenite lamellae from orthopyroxene megacrysts was followed by late veins of clinopyroxene, andesine, and almandine garnet, and then by widespread alteration of orthopyroxene to talc and dispersed magnetite. Tschermakitic hornblende was replaced by magnesio-hornblende. Both orthopyroxene and amphibole megacrysts have corona rims of magnesio-hornblende, biotite, and chlorite.
  4. The magnetite-ilmenite ore, containing minor Fe-sulfides, formed from an immiscible magma that inmixed some siliceous material.
  5. The Steel Mountain anorthosite massif shows polybaric evolution of a rising mush of plagioclase crystals. The magnetite-ilmenite ore contains inclusions of olivine and of pargasite that equilibrated at >30 km depth. Orthopyroxene megacrysts and groundmass crystallized at 20–25 km and amphibole megacrysts at 15–20 km. The corona rims equilibrated at upper crustal depths.
  6. Sm-Nd isotopes and Ar-Ar geochronology are more consistent with a peri-Gondwanan than a peri-Laurentian origin of the Steel Mountain complex.
  7. Zircon is rare or absent in the anorthosite and gabbro. Common zircon in this study is found only in a post-tectonic, altered, mafic dyke.

**Supplementary Materials:** The following supporting information can be downloaded at: <https://www.mdpi.com/article/10.3390/min14010081/s1>, Figure S1: BSE images, sample 8174. Table S1: EDS mineral analyses, sample 8174. Table S2: Ar-Ar dating.

**Author Contributions:** Conceptualization, G.P.-P.; methodology, G.P.-P.; investigation, G.D., G.P.-P. and D.J.W.P.; resources, G.P.-P.; data curation, G.P.-P.; writing—original draft preparation, G.P.-P., G.D. and D.J.W.P.; writing—review and editing, D.J.W.P.; supervision, G.P.-P.; project administration, G.P.-P.; funding acquisition, G.P.-P. All authors have read and agreed to the published version of the manuscript.

**Funding:** This research was funded by the Natural Sciences and Engineering Research Council of Canada (NSERC) discovery grants to G. Pe-Piper, most recently grant no. 2016-04310. Geological Survey of Canada contribution number 20230349.

**Data Availability Statement:** Data are available in an Open File Report [14].

**Acknowledgments:** We thank Doug Archibald and Dan Kontak for the Ar-Ar date.

**Conflicts of Interest:** The authors declare no conflicts of interest. The funders had no role in the design of the study; in the collection, analyses, or interpretation of data; in the writing of the manuscript; or in the decision to publish the results.

## References

1. Lin, S.; Brem, A.G.; van Staal, C.R.; Davis, D.W.; McNicoll, V.J.; Pehrsson, S. The Corner Brook Lake block in the Newfoundland Appalachians: A suspect terrane along the Laurentian margin and evidence for large-scale orogen-parallel motion. *GSA Bull.* **2013**, *125*, 1618–1632. [\[CrossRef\]](#)
2. Martin, A.J.; Bosbyshell, H. Further detrital zircon evidence for peri-Gondwanan blocks in the central Appalachian Piedmont Province, USA. *Can. J. Earth Sci.* **2019**, *56*, 1061–1076. [\[CrossRef\]](#)
3. Currie, K.L.; van Berkel, J.T. Notes to Accompany a Geological Map of the Southern Long Range, southwestern Newfoundland. *Geol. Surv. Can. Pap.* **1992**, *91–10*, 1–10.
4. Ashwal, L.D.; Bybee, G.M. Crystal evolution and the temporality of anorthosites. *Earth-Sci. Rev.* **2017**, *173*, 307–330. [\[CrossRef\]](#)
5. Emslie, R.F. Pyroxene megacrysts from anorthositic rocks. New clues to the sources and evolution of the parent magmas. *Can. Mineral.* **1975**, *13*, 138–145.
6. Heinonen, A.; Kivisaari, H.; Michallik, R.M. High-aluminum orthopyroxene megacrysts (HAOM) in the Ahvenisto complex, SE Finland, and the polybaric crystallization of massif-type anorthosites. *Contrib. Min. Pet.* **2020**, *175*, 10. [\[CrossRef\]](#)
7. Owens, B.E.; Rockow, M.W.; Dymek, R.F. Jotunites from the Grenville province, Quebec: Petrological characteristics and implications for massif anorthosite petrogenesis. *Lithos* **1993**, *30*, 57–80. [\[CrossRef\]](#)
8. Owens, B.E.; Dymek, R.F. Significance of pyroxene megacrysts for massif anorthosite petrogenesis: Constraints from the Labrieville, Quebec, pluton. *Am. Mineral.* **1995**, *80*, 144–161. [\[CrossRef\]](#)

9. Veblen, D.R.; Bish, D.L. TEM and X-ray study of orthopyroxene megacrysts: Microstructures and crystal chemistry. *Am. Mineral.* **1988**, *73*, 677–691.
10. Feininger, T. Geology and geophysics of the ‘type’ anorthosite, Chateau-Richer, Quebec. *Can. Mineral.* **1993**, *31*, 849–859.
11. Van Berkel, J.T. Geology of the Dashwoods Pond, St. Fintan’s and Main Gut map areas, southwest Newfoundland. *Geol. Surv. Can. Pap.* **1987**, *87-1A*, 399–408.
12. Collins, P.G. A Petrographic and Geochemical Characterization and the Evaluation of the Exploration Potential for Nickel Sulfides in Several Mafic-Ultramafic Intrusive Complexes in Newfoundland. Master’s Thesis, Memorial University, St John’s, NL, Canada, 2007.
13. Baird, D.M. The magnetite and gypsum deposits of the Sheep Brook-Lookout Brook area. *Geol. Surv. Can. Bull.* **1954**, *27*, 20–40.
14. Pe-Piper, G.; Dessureau, G. The West Moose River anorthosites, Avalon zone, Nova Scotia. *Geol. Surv. Can. Open File Rep.* **2002**, *4188*, 1–140.
15. Pe-Piper, G.; Piper, D.J.W.; Matarangas, D. Regional implications of geochemistry and style of emplacement of Miocene I-type diorite and granite, Delos, Cyclades, Greece. *Lithos* **2002**, *60*, 47–66. [[CrossRef](#)]
16. Erdmer, P.; Ghent, E.D.; Archibald, D.A.; Stout, M.Z. Paleozoic and Mesozoic high-pressure metamorphism at the margin of ancestral North America in central Yukon. *GSA Bull.* **1998**, *110*, 615–629. [[CrossRef](#)]
17. Warr, L.N. IMA–CNMNC approved mineral symbols. *Mineral. Mag.* **2021**, *85*, 291–320. [[CrossRef](#)]
18. Deer, W.A.; Howie, R.A.; Zussman, J. *Rock-Forming Minerals*; Longmans: London, UK, 1963.
19. Anderson, J.L.; Smith, D.R. The effects of temperature and fO<sub>2</sub> on the Al-in-hornblende barometer. *Am. Mineral.* **1995**, *80*, 549–559. [[CrossRef](#)]
20. Leake, B.E.; Woolley, A.R.; Arps, C.E.; Birch, W.D.; Gilbert, M.C.; Grice, J.D.; Hawthorne, F.C.; Kato, A.; Kisch, H.J.; Krivovichev, V.G.; et al. Nomenclature of amphiboles. *Can. Mineral.* **1997**, *35*, 219–246.
21. Sun, S.S.; McDonough, W.F. Chemical and isotopic systematics of oceanic basalts: Implications for mantle composition and processes. *Geol. Soc. Lond. Spec. Publ.* **1989**, *42*, 313–345. [[CrossRef](#)]
22. Cashman, K.V.; Sparks, R.S.J.; Blundy, J.D. Vertically extensive and unstable magmatic systems: A unified view of igneous processes. *Science* **2017**, *355*, 3055. [[CrossRef](#)]
23. Higgins, M.D. Textural coarsening in igneous rocks. *Int. Geol. Rev.* **2011**, *53*, 354–376. [[CrossRef](#)]
24. Polat, A.; Appel, P.W.; Fryer, B.; Windley, B.; Frei, R.; Samson, I.M.; Huang, H. Trace element systematics of the Neoproterozoic Fiskensset anorthosite complex and associated meta-volcanic rocks, SW Greenland: Evidence for a magmatic arc origin. *Precambrian Res.* **2009**, *175*, 87–115. [[CrossRef](#)]
25. Lister, G.F. The composition and origin of selected iron-titanium deposits. *Econ. Geol.* **1966**, *61*, 275–310. [[CrossRef](#)]
26. Chivas, A.R. Geochemical evidence for magmatic fluids in porphyry copper mineralization. Part I. Mafic silicates from the Koloula Igneous Complex. *Contrib. Min. Pet.* **1981**, *78*, 389–403. [[CrossRef](#)]
27. Dymek, R.F.; Gromet, L.P. Nature and origin of orthopyroxene megacrysts from the St. Urbain anorthosite massif, Quebec. *Can. Mineral.* **1984**, *22*, 297–326.
28. Zimmer, M.M.; Plank, T.; Hauri, E.H.; Yogodzinski, G.M.; Stelling, P.; Larsen, J.; Singer, B.; Jicha, B.; Mandeville, C.; Nye, C.J. The role of water in generating the calc-alkaline trend: New volatile data for Aleutian magmas and a new tholeiitic index. *J. Petrol.* **2010**, *51*, 2411–2444. [[CrossRef](#)]
29. Hinchey, A.M.; Knight, I.; Sandeman, H.A.; Hinchey, J.G. Tournaisian volcanism associated with transtensional basin development in western Newfoundland during the amalgamation of Pangea. *Gondwana Res.* **2022**, *110*, 226–248. [[CrossRef](#)]
30. Hendriks, M.; Jamieson, R.A.; Willett, S.D.; Zentilli, M. Burial and exhumation of the Long Range Inlier and its surroundings, western Newfoundland: Results of an apatite fission-track study. *Can. J. Earth Sci.* **1993**, *30*, 1594–1606. [[CrossRef](#)]
31. van Staal, C.R.; Barr, S.M. Lithospheric architecture and tectonic evolution of the Canadian Appalachians and associated Atlantic margin. *Geol. Assoc. Can. Spec. Pap.* **2012**, *49*, 55–95.
32. van Staal, C.R.; Barr, S.M.; McCausland, P.J.A.; Thompson, M.D.; White, C.E. Tonian–Ediacaran tectonomagmatic evolution of West Avalonia and its Ediacaran–early Cambrian interactions with Ganderia: An example of complex terrane transfer due to arc–arc collision? *Geol. Soc. Lond. Spec. Publ.* **2021**, *503*, 143–167. [[CrossRef](#)]
33. Pollock, J.C.; Hibbard, J.P.; van Staal, C.R. A paleogeographical review of the peri-Gondwanan realm of the Appalachian orogen. *Can. J. Earth Sci.* **2012**, *49*, 259–288. [[CrossRef](#)]
34. Waldron, J.W.G.; Schofield, D.I.; Murphy, J.B. Diachronous Paleozoic accretion of peri-Gondwanan terranes at the Laurentian margin. *Geol. Soc. Lond. Spec. Publ.* **2019**, *470*, 289–310. [[CrossRef](#)]

**Disclaimer/Publisher’s Note:** The statements, opinions and data contained in all publications are solely those of the individual author(s) and contributor(s) and not of MDPI and/or the editor(s). MDPI and/or the editor(s) disclaim responsibility for any injury to people or property resulting from any ideas, methods, instructions or products referred to in the content.